The Astrophysical Journal, 709:159–167, 2010 January 20 doi:10.1088/0004-637X/709/1/159

WASP-17b: AN ULTRA-LOW DENSITY PLANET IN A PROBABLE RETROGRADE ORBIT*

D. R. Anderson[1], C. Hellier[1], M. Gillon[2,3], A. H. M. J. Triaud[2], B. Smalley[1], L. Hebb[4], A. Collier Cameron[4], P. F. L. Maxted[1], D. Queloz[2], R. G. West[5], S. J. Bentley[1], B. Enoch[4], K. Horne[4], T. A. Lister[6], M. Mayor[2], N. R. Parley[4], F. Pepe[2], D. Pollacco[7], D. Ségransan[2], S. Udry[2], and D. M. Wilson[1,8]

[1] Astrophysics Group, Keele University, Staffordshire, ST5 5BG, UK; dra@astro.keele.ac.uk
[2] Observatoire de Genève, Université de Genève, 51 Chemin des Maillettes, 1290 Sauverny, Switzerland
[3] Institut d'Astrophysique et de Géophysique, Université de Liège, Allée du 6 Août, 17, Bat. B5C, Liège 1, Belgium
[4] School of Physics and Astronomy, University of St. Andrews, North Haugh, Fife, KY16 9SS, UK
[5] Department of Physics and Astronomy, University of Leicester, Leicester, LE1 7RH, UK
[6] Las Cumbres Observatory, 6740 Cortona Dr. Suite 102, Santa Barbara, CA 93117, USA
[7] Astrophysics Research Centre, School of Mathematics & Physics, Queen's University, University Road, Belfast, BT7 1NN, UK
Received 2009 August 11; accepted 2009 November 30; published 2009 December 29

ABSTRACT

We report the discovery of the transiting giant planet WASP-17b, the least-dense planet currently known. It is 1.6 Saturn masses, but 1.5–2 Jupiter radii, giving a density of 6%–14% that of Jupiter. WASP-17b is in a 3.7 day orbit around a sub-solar metallicity, $V = 11.6$, F6 star. Preliminary detection of the Rossiter–McLaughlin effect suggests that WASP-17b is in a retrograde orbit ($\lambda \approx -150°$), indicative of a violent history involving planet–planet or star–planet scattering. WASP-17b's bloated radius could be due to tidal heating resulting from recent or ongoing tidal circularization of an eccentric orbit, such as the highly eccentric orbits that typically result from scattering interactions. It will thus be important to determine more precisely the current orbital eccentricity by further high-precision radial velocity measurements or by timing the secondary eclipse, both to reduce the uncertainty on the planet's radius and to test tidal-heating models. Owing to its low surface gravity, WASP-17b's atmosphere has the largest scale height of any known planet, making it a good target for transmission spectroscopy.

Key words: planetary systems – stars: individual (WASP-17)

Online-only material: color figures, machine-readable table

1. INTRODUCTION

The first measurement of the radius and density of an extrasolar planet was made when HD 209458b was seen to transit its parent star (Charbonneau et al. 2000; Henry et al. 2000). The large radius (1.32 $R_{\rm Jup}$) of HD 209458b, confirmed by later observations (e.g., Knutson et al. 2007), could not be explained by standard models of planet evolution (Guillot & Showman 2002). Since the discovery of HD 209458b, other bloated planets have been found, including TrES-4 (Mandushev et al. 2007), WASP-12b (Hebb et al. 2008), WASP-4b (Wilson et al. 2008; Gillon et al. 2009a, Winn et al. 2009a, Southworth et al. 2009), WASP-6b (Gillon et al. 2009b), XO-3b (Johns-Krull et al. 2008; Winn et al. 2008), and HAT-P-1b (Bakos et al. 2007; Winn et al. 2007; Johnson et al. 2008). Of these, TrES-4 is the most bloated, with a density 15% that of Jupiter, and a radius larger by a factor 1.78 (Sozzetti et al. 2009).

The mass, composition, and evolution history of a planet determines its current radius (e.g., Burrows et al. 2007; Fortney et al. 2007). Recently, numerous theoretical studies have attempted to discover the reasons why some short-orbit, giant planets are bloated. A small fraction of stellar insolation energy would be sufficient to account for bloating, but no known mechanism is able to transport the insolation energy deep enough within a planet to significantly affect the planet's evolution (Guillot & Showman 2002; Burrows et al. 2007). Enhanced atmospheric opacity would cause internal heat to be lost more slowly, causing a planet's radius to be larger than otherwise at a given age (Burrows et al. 2007). Indeed, the more highly irradiated planets are thought to have enhanced opacity due to species such as gas-phase TiO/VO, tholins or polyacetylenes (Burrows et al. 2008; Fortney et al. 2008). These upper-atmosphere absorbers result in detectable stratospheres (e.g., Knutson et al. 2009) and prevent incident flux from reaching deep into the atmosphere, causing a large day–night temperature contrast, which leads to faster cooling (Guillot & Showman 2002). That some planets are not bloated, though they are in similar irradiation environments and have otherwise similar properties to bloated planets, may be due to differences in evolution history or in core mass (Guillot et al. 2006; Burrows et al. 2007).

Currently, the most promising explanation for the large radii of some planets is that they were inflated when the tidal circularization of eccentric orbits caused energy to be dissipated as heat within the planets (Bodenheimer et al. 2001; Gu et al. 2003; Jackson et al. 2008a; Ibgui & Burrows 2009). Indeed, Jackson et al. (2008b) found that the distribution of the eccentricities of short-orbit ($a < 0.2$ AU) planets could have evolved, via tidal circularization, from a distribution identical to that of the farther-out planets.

The angular momenta of a star and its planets derive from that of their parent molecular cloud, so close alignment is expected between the stellar spin and planetary orbit axes. When a planet obscures a portion of its parent star, we observe an apparent spectroscopic redshift or blueshift, which we see depends on whether the area obscured is approaching or receding relative to the star's bulk motion. This manifests as an "anomalous" radial velocity (RV) and is known as the Rossiter–McLaughlin (RM) effect (e.g., Queloz et al. 2000a; Gaudi & Winn 2007).

* Based in part on data collected with the HARPS spectrograph at ESO La Silla Observatory under programme ID 081.C-0388(A).
[8] Current address: Centre for Astrophysics & Planetary Science, University of Kent, Canterbury, Kent, CT2 7NH, UK.

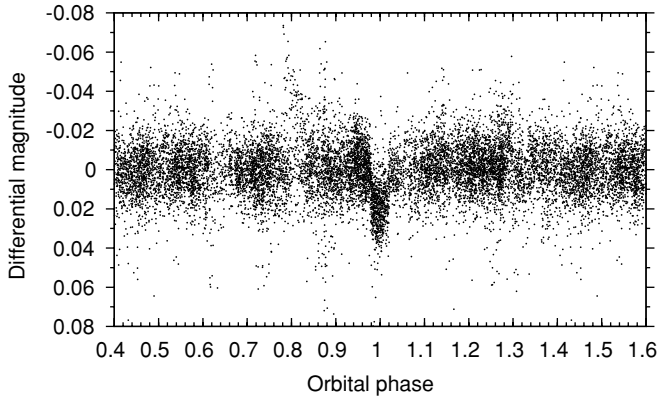

Figure 1. WASP-South discovery light curve, phase-folded with the ephemeris of Table 4. Points with error > 0.05 mag ($3\sigma_{\rm median}$) were clipped for display. From the WASP discovery photometry, we found a high probability (0.74) of WASP-17 being a main-sequence star and a zero probability of the companion having $R_{\rm P} < 1.5\ R_{\rm Jup}$ (Collier Cameron et al. 2007). As such, the system did not fulfill one of our usual selection criteria, $\mathcal{P}(R_P < 1.5\ R_{\rm Jup}) > 0.2$, for follow-up spectroscopy (Collier Cameron et al. 2007). We therefore advise other transit surveys to exercise caution in rejecting candidates on the basis of size, so as not to miss interesting systems like WASP-17.

The shape of the RM effect is sensitive to the path a planet takes across its parent star, relative to the star's spin axis. Thus, spectroscopic observation of a transit allows measurement of λ, the sky-projected angle between the stellar spin, and planetary orbit axes. Short-orbit, giant planets are thought to have formed just outside the ice boundary and migrated inward (e.g., Ida & Lin 2004). Thus, λ is a useful diagnostic for theories of planet migration, some of which predict preservation of initial spin–orbit alignment and some of which would occasionally produce large misalignments. For example, migration via tidal interaction of a giant planet with a gas disk (Lin et al. 1996; Ward 1997) is expected to preserve spin–orbit alignment, whereas migration via a combination of planet–planet scattering and tidal circularization of a resultant eccentric orbit is able to produce a significant misalignment (e.g., Rasio & Ford 1996; Chatterjee et al. 2008; Nagasawa et al. 2008). To date, λ has been determined for 14 systems (Fabrycky & Winn 2009; Gillon 2009; Triaud et al. 2009) and for three of these a significant misalignment was found: XO-3b ($\lambda = 37.3 \pm 3.7$ deg, Winn et al. 2009b; see also: Hébrard et al. 2008), HD 80606b ($\lambda = 59^{+28}_{-18}$ deg, Gillon 2009; see also: Moutou et al. 2009; Pont et al. 2009; Winn et al. 2009c), and WASP-14b ($\lambda = -33.1 \pm 7.4$ deg, Johnson et al. 2009; see also: Joshi et al. 2009).

In this paper, we present the discovery of the transiting extrasolar planet WASP-17b, which is the least-dense planet currently known and the first planet found to be in a probable retrograde orbit.

2. OBSERVATIONS

WASP-17 is a $V = 11.6$, F6 star in Scorpius. It was observed by WASP-South (Pollacco et al. 2006) from 2006 May 4 to August 18, again from 2007 March 5 to August 19 and again from 2008 March 2 to April 19. These observations resulted in 15,509 usable photometric measurements, spanning two years and from two separate fields. A transit search (Collier Cameron et al. 2006) found a strong, 3.7 day periodicity (Figure 1).

A full transit of WASP-17 was observed in the I_c band with EulerCAM on the 1.2 m Euler–Swiss telescope on 2008 May 6. The telescope was defocused to give a mean stellar profile width of 4″. Over a duration of 6 hr, 181 frames were obtained with a range of exposure times of 32–98 s—the exposure time was tuned to keep the stellar peaks constant. Observations began when WASP-17 was at air mass 1.07; the star then passed through the meridian before reaching air mass 1.8 when observations ended at twilight. The resulting light curve and the residuals about the model fits (Section 4) are shown in Figure 2, and the photometry is given in Table 1.

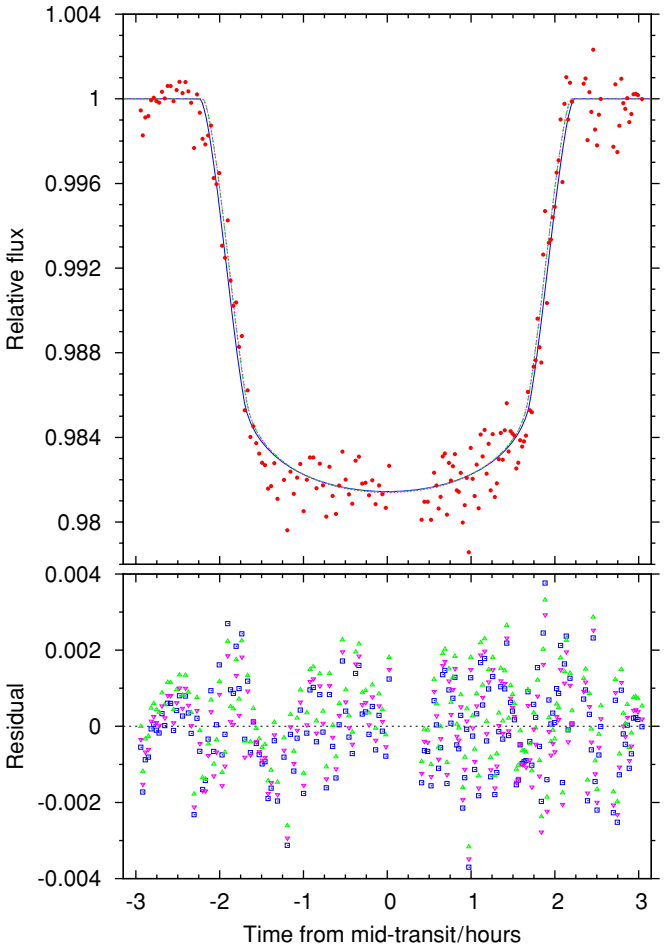

Figure 2. Upper panel: Euler I_c-band light curve (red circles) taken on 2008 May 6. Overplotted are the best-fitting model transits (lines; Section 4) from the parameters of Table 4; consult that table for the key to the color and symbol scheme. Lower panel: residuals about the model fits. For the green and the magenta models (triangles) the noise is the same (rms = 1140 ppm; red noise = 840 ppm—calculated using the method of Gillon et al. 2006); for the blue model (squares) the noise is slightly higher (rms = 1210 ppm; red noise = 920 ppm, Gillon et al. 2006). The mean theoretical error is 800 ppm.

(A color version of this figure is available in the online journal.)

Table 1
I_c-band Photometry of WASP-17

HJD (days)	Relative Flux	$\sigma_{\rm flux}$
2454592.677426	0.999803	0.000959
2454592.678457	0.998623	0.000956
2454592.679703	0.999471	0.000670
...	...	...
2454592.923564	1.00053	0.00141
2454592.926643	1.00034	0.00145

(This table is available in its entirety in a machine-readable form in the online journal. A portion is shown here for guidance regarding its form and content.)

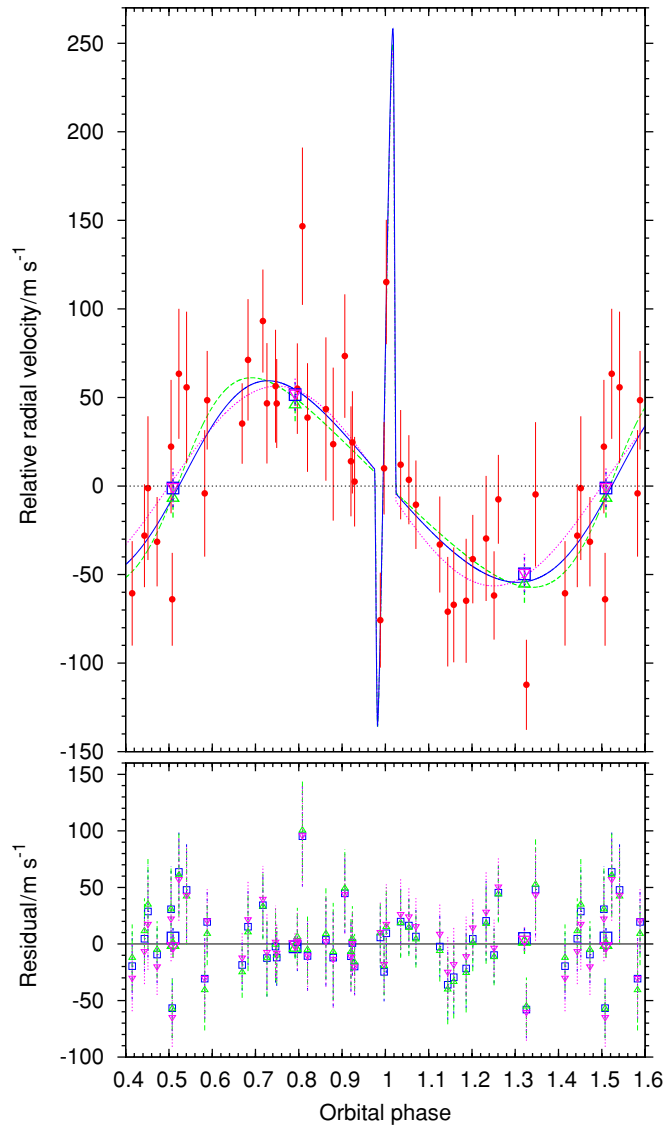

Figure 3. Upper panel: relative RV measurements of WASP-17 as measured by CORALIE (red circles). The three, color-coded solid lines are the model orbital solutions (Section 4) based on the parameters of Table 4 and incorporate the RM effect. As the zero-point offset between HARPS and CORALIE is a free parameter in the models, the HARPS measurements are shown once per model, with corresponding symbols and colors (Table 4). The center-of-mass velocities of Table 4 have been subtracted. Lower panel: residuals about the model solutions; consult Table 4 for the key to the symbol and color scheme.

(A color version of this figure is available in the online journal.)

Table 2
Radial Velocity Measurements of WASP-17

BJD–2 450 000	RV (km s^{-1})	σ_{RV} (km s^{-1})	BS[a] (km s^{-1})
CORALIE:			
4329.6037	−49.4570	0.0428	0.0829
4360.4863	−49.3661	0.0444	0.1290
4362.4980	−49.5175	0.0407	0.1335
4364.4880	−49.4891	0.0432	−0.0213
4367.4883	−49.4415	0.0343	0.1931
4558.8839	−49.4988	0.0311	−0.0101
4559.7708	−49.5798	0.0325	−0.0229
4560.7314	−49.5734	0.0295	0.0303
4588.7799	−49.4881	0.0289	−0.0638
4591.7778	−49.4661	0.0340	−0.0631
4622.6917	−49.3976	0.0351	0.1071
4624.6367	−49.4494	0.0367	0.2581
4651.6195	−49.4564	0.0319	0.0459
4659.5246	−49.4693	0.0405	0.0972
4664.6425	−49.5424	0.0353	0.0401
4665.6593	−49.4905	0.0377	0.0770
4682.5824	−49.5007	0.0309	0.0707
4684.6264	−49.5169	0.0357	−0.0418
4685.5145	−49.4741	0.0307	−0.0393
4690.6182	−49.5776	0.0350	0.0541
4691.6077	−49.5140	0.0406	−0.0380
4939.8457	−49.4394	0.0349	0.1127
4940.7346	−49.5838	0.0309	0.0777
4941.8520	−49.5408	0.0290	0.0163
4942.6959	−49.4775	0.0227	0.1030
4942.8747	−49.4196	0.0291	−0.0355
4943.6655	−49.5103	0.0253	0.1504
4943.8872	−49.5885	0.0268	0.0732
4944.6858	−49.5540	0.0250	0.0951
4944.8689	−49.5746	0.0249	0.0694
4945.6969	−49.5442	0.0252	0.0727
4945.8277	−49.5767	0.0263	0.0579
4946.7289	−49.4662	0.0251	0.0351
4946.9069	−49.4578	0.0256	0.0326
4947.6558	−49.5028	0.0261	−0.1128
4947.8694	−49.5092	0.0251	0.0614
4948.6415	−49.5203	0.0251	0.1043
4948.8836	−49.6250	0.0254	−0.0153
4949.8646	−49.4643	0.0279	0.0307
4951.6661	−49.5233	0.0250	−0.1208
4951.8719	−49.5458	0.0271	−0.0061
HARPS:			
4564.8195	−49.4884	0.0108	−0.0239
4565.8731	−49.4356	0.0092	−0.0103
4567.8516	−49.5368	0.0105	−0.0015

Note. [a] BS: bisector span.

Using the CORALIE spectrograph mounted on the Euler–Swiss telescope (Baranne et al. 1996; Queloz et al. 2000b), five spectra of WASP-17 were obtained in 2007, 16 more in 2008, and a further 20 in 2009. Three high-precision spectra were obtained in 2008 with the HARPS spectrograph (Mayor et al. 2003), based on the 3.6 m ESO telescope. RV measurements were computed by weighted cross-correlation (Baranne et al. 1996; Pepe et al. 2005) with a numerical G2-spectral template. RV variations were detected with the same period found from the WASP photometry and with semi-amplitude of ∼50 m s^{-1}, consistent with a planetary-mass companion. The RV measurements are listed in Table 2 and are plotted in Figure 3.

To test the hypothesis that the RV variations are due to spectral line distortions caused by a blended eclipsing binary, a line-bisector analysis (Queloz et al. 2001) of the CORALIE and HARPS cross-correlation functions was performed. The lack of correlation between bisector span and RV (Figure 4), especially for the high-precision HARPS measurements, supports the identification of the transiting body as a planet.

3. STELLAR PARAMETERS

The combined CORALIE and HARPS spectra from 2007–2008, co-added into 0.01 Å steps, give a signal-to-noise ratio of ∼100:1. The stellar parameters and elemental abundances of WASP-17 were determined using spectrum synthesis and equivalent-width measurements (Gillon et al. 2009b; West et al. 2009) and are given in Table 3. In the spectra, the Li I 6708 Å line is not detected (EW < 2 mÅ), giving an upper-limit on the

Table 3
Stellar Parameters of WASP-17

Parameters	Values
$T_{\rm eff}$ (K)	6550 ± 100
log g_* (cgs)	4.2 ± 0.2
$\xi_{\rm t}$ (km s^{-1})	1.6 ± 0.2
$v \sin i$ (km s^{-1})	9.0 ± 1.5
Spectral Type	F6
[Na/H]	−0.15 ± 0.06
[Mg/H]	−0.21 ± 0.07
[Al/H]	−0.38 ± 0.05
[Si/H]	−0.18 ± 0.09
[Ca/H]	−0.08 ± 0.14
[Sc/H]	−0.20 ± 0.14
[Ti/H]	−0.20 ± 0.12
[V/H]	−0.38 ± 0.13
[Cr/H]	−0.23 ± 0.14
[Fe/H]	−0.25 ± 0.09
[Ni/H]	−0.32 ± 0.11
log N(Li)	< 1.3
v (mag)	11.6
Distance (pc)	400 ± 60

Notes. R.A. (J2000) = $15^{\rm h}59^{\rm m}50\overset{\rm s}{.}94$; Decl. (J2000) = $-28^\circ03'42\overset{''}{.}3$; 1SWASP J155950.94 − 280342.3; USNO-B1.0 0619-0419495; 2MASS 15595095 − 2803422.

Lithium abundance of log n(Li/H) + 12 < 1.3. However, the effective temperature of this star implies that it is in the lithium gap (Böhm-Vitense 2004) and so the lithium abundance does not provide an age constraint. In determining the projected stellar rotation velocity ($v \sin i$) from the HARPS spectra, a value for macroturbulence ($v_{\rm mac}$) of 6 km s^{-1} was adopted (Gray 2008, p. 507) and an instrumental FWHM of 0.06 Å, determined from the telluric lines around 6300 Å, was used. A best-fitting value of $v \sin i = 9.0 \pm 1.5$ km s^{-1} was obtained. However, if $v_{\rm mac}$ is lower than the assumed 6 km s^{-1} then $v \sin i$ would be slightly higher, with a value of 11 km s^{-1} obtained if $v_{\rm mac}$ is assumed to be zero.

We attempted to measure the rotation period of WASP-17 by searching for sinusoidal, rotational modulation of the WASP light curve (Hebb et al. 2010), as may be induced by a non-axisymmetric distribution of starspots. Considering periods of 1.05–30 days, the best-fitting period is 24.7 days. However, the amplitudes of the phase-folded light curves from each camera from each season are small (2–8 mmag). Assuming spin–orbit alignment, with $v \sin i = 9.0$ km s^{-1}, and using the values of stellar radius given in Table 4 (see Section 4), a stellar rotation period of 8.5–11 days is expected.

We estimated the distance of WASP-17 (400 ± 60 pc) using the distance modulus, the TYCHO apparent visual magnitude ($V = 11.6$) and the absolute visual magnitude of an F6V star ($V = 3.6$; Gray 2008, p. 507); we assumed $E(B - V) = 0$.

4. SYSTEM PARAMETERS

The WASP-South and EulerCAM photometry were combined with the CORALIE and HARPS RV measurements in a simultaneous Markov-chain Monte Carlo (MCMC) analysis (Collier Cameron et al. 2007; Pollacco et al. 2008). The proposal parameters we use are: $T_{\rm c}$, P, ΔF, T_{14}, b, K_1, M_*, $e \cos\omega$, $e \sin\omega$, $v \sin i \cos\lambda$, and $v \sin i \sin\lambda$. Here $T_{\rm c}$ is the epoch of mid-transit, P is the orbital period, ΔF is the fractional flux deficit that would be observed during transit in the absence of limb darkening, T_{14} is the total transit duration (from first to fourth contact), b is the impact parameter of the planet's path across the stellar disk, K_1 is the stellar reflex velocity semi-amplitude, M_* is the stellar mass, e is the orbital eccentricity, and ω is the argument of periastron.

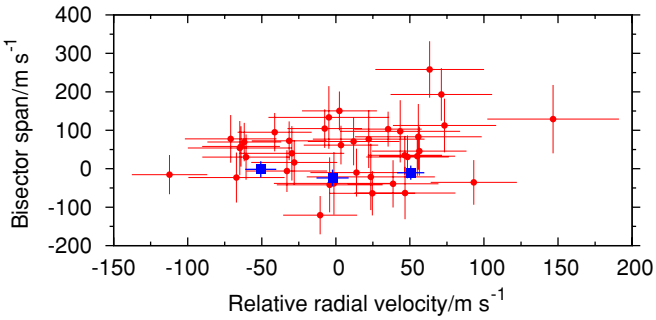

Figure 4. Bisector span vs. relative RV for the CORALIE (red circles) and HARPS (blue squares) spectra. Averages of the center-of-mass velocities and zero-point offsets of Table 4 were subtracted. Bisector uncertainties equal to twice the RV uncertainties have been adopted. The Pearson correlation coefficient is 0.19.

(A color version of this figure is available in the online journal.)

At each step in the MCMC procedure, each proposal parameter is perturbed from its previous value by a small, random amount. From the proposal parameters, model light and RV curves are generated, and χ^2 is calculated from their comparison with the data. A step is accepted if χ^2 is lower than for the previous step; a step with higher χ^2 may also be accepted, the probability for which is lower for larger $\Delta\chi^2$. In this way, the parameter space around the optimum solution is thoroughly explored. Provided the probability of accepting a step of higher χ^2 is chosen correctly, the distribution of points for an MCMC chain gives the standard errors on the parameters (e.g., Ford 2006).

We place a prior on M_* that, via a Bayesian penalty, causes its values in accepted MCMC steps to approximate a Gaussian distribution with mean M_0 and standard deviation $\sigma_{\rm M} = 0.1\ M_0$, where M_0 is the initial estimate of M_*. To determine M_0 and to estimate the star's age, an evolutionary analysis (Hebb et al. 2008) was performed. In that, an initial MCMC run was used to determine the stellar density, which depends on the shape of the transit light curve and the eccentricity of the orbit. The stellar evolution tracks of Girardi et al. (2000) were then interpolated using this stellar density and using the stellar temperature and metallicity from the spectral analysis (Figure 5). This suggests that WASP-17 has evolved off the zero-age main sequence, with a mass of $1.20^{+0.10}_{-0.11}\ M_\odot$ and an age of $3.0^{+0.9}_{-2.6}$ Gyr. This stellar mass was used as the initial estimate, M_0, in the MCMC solution (Case 1) presented in the second column of Table 4. The best-fitting eccentricity is non-zero at the 2σ level ($e = 0.129^{+0.106}_{-0.068}$; $\omega = 290^{\circ}{}^{+106}_{-16}$ deg). The best-fitting planet radius is large but uncertain ($R_{\rm P} = 1.74^{+0.26}_{-0.23}\ R_{\rm Jup}$). This uncertainty results from e and ω being poorly constrained by the RV data, causing the velocity of the planet during transit, and therefore the distance traveled (i.e., the stellar radius), to be uncertain. The planet radius is related to the stellar radius by the measured depth of transit, so it too is uncertain.

The stellar age from the first MCMC solution and $v \sin i$ from the spectral analysis are consistent with WASP-17 being young. As such, a second MCMC analysis was performed, with a main sequence (MS) prior on the star and with eccentricity a free parameter. With the MS prior, a Bayesian penalty ensures that,

Table 4
System Parameters of WASP-17

Parameter	Case 1 (adopted)	Case 2	Case 3
Extra constraints	...	MS prior	$e = 0$
Graph color	Blue	Green	Magenta
Graph symbol	Squares	Upward triangles	Downward triangles
Graph line	Solid	Dashed	Dotted
Stellar age (Gyr)	$3.0^{+0.9}_{-2.6}$	$1.2^{+2.8}_{-1.2}$	$3.1^{+1.1}_{-0.8}$
P (days)	$3.7354417^{+0.0000072}_{-0.0000073}$	$3.7354417^{+0.0000073}_{-0.0000074}$	$3.7354414^{+0.0000074}_{-0.0000074}$
T_c (HJD)	$2454559.18102^{+0.00028}_{-0.00028}$	$2454559.18100^{+0.00027}_{-0.00028}$	$2454559.18096^{+0.00028}_{-0.00028}$
T_{14} (days)	$0.1822^{+0.0019}_{-0.0023}$	$0.1825^{+0.0017}_{-0.0017}$	$0.1824^{+0.0016}_{-0.0016}$
$T_{12} = T_{34}$ (days)	$0.0235^{+0.0019}_{-0.0030}$	$0.0236^{+0.0017}_{-0.0018}$	$0.0239^{+0.0017}_{-0.0017}$
$\Delta F = R_P^2/R_*^2$	$0.01672^{+0.00029}_{-0.00035}$	$0.01674^{+0.00027}_{-0.00027}$	$0.01678^{+0.00026}_{-0.00027}$
$b \equiv a \cos i/R_*$	$0.352^{+0.075}_{-0.316}$	$0.355^{+0.068}_{-0.111}$	$0.370^{+0.064}_{-0.096}$
K_1 (km s^{-1})	$0.0569^{+0.0055}_{-0.0053}$	$0.0592^{+0.0058}_{-0.0057}$	$0.0564^{+0.0051}_{-0.0051}$
γ (km s^{-1})	$-49.5128^{+0.0016}_{-0.0016}$	$-49.5128^{+0.0014}_{-0.0014}$	$-49.5125^{+0.0014}_{-0.0015}$
$\gamma_{\rm HARPS} - \gamma_{\rm COR.}$ (km s^{-1})	$0.0267^{+0.0034}_{-0.0035}$	$0.0297^{+0.0023}_{-0.0023}$	$0.0233^{+0.0015}_{-0.0015}$
a (AU)	$0.0501^{+0.0017}_{-0.0018}$	$0.0494^{+0.0017}_{-0.0018}$	$0.0507^{+0.0017}_{-0.0018}$
i (deg)	$87.8^{+2.0}_{-1.0}$	$88.16^{+0.58}_{-0.45}$	$86.95^{+0.87}_{-0.63}$
$e \cos \omega$	$0.036^{+0.034}_{-0.031}$	$0.034^{+0.025}_{-0.024}$	...
$e \sin \omega$	$-0.10^{+0.13}_{-0.13}$	$-0.233^{+0.071}_{-0.070}$	...
e	$0.129^{+0.106}_{-0.068}$	$0.237^{+0.068}_{-0.069}$	0. (fixed)
ω (deg)	290^{+106}_{-16}	$278.0^{+8.2}_{-5.6}$	...
$\phi_{\rm mid\text{-}eclipse}$	$0.523^{+0.021}_{-0.020}$	$0.522^{+0.016}_{-0.015}$	0.5 (fixed)
T_{58} (days)[a]	$0.152^{+0.040}_{-0.034}$	$0.117^{+0.017}_{-0.015}$	$0.1824^{+0.0016}_{-0.0016}$ (fixed)
$T_{56} = T_{78}$ (days)[b]	$0.0186^{+0.0063}_{-0.0046}$	$0.0140^{+0.0022}_{-0.0019}$	$0.0239^{+0.0017}_{-0.0017}$ (fixed)
λ (deg)	-147^{+49}_{-11}	$-148.7^{+13.7}_{-9.3}$	$-149.3^{+11.5}_{-8.9}$
$v \sin i$ (km s^{-1})	$20.0^{+69.2}_{-5.2}$	$19.1^{+5.7}_{-4.8}$	$19.1^{+5.3}_{-4.7}$
M_* ($M_\odot$)	$1.20^{+0.12}_{-0.12}$	$1.16^{+0.12}_{-0.12}$	$1.25^{+0.13}_{-0.13}$
R_* ($R_\odot$)	$1.38^{+0.20}_{-0.18}$	$1.200^{+0.081}_{-0.080}$	$1.566^{+0.073}_{-0.073}$
$\log g_*$ (cgs)	$4.23^{+0.12}_{-0.12}$	$4.341^{+0.068}_{-0.068}$	$4.143^{+0.032}_{-0.031}$
ρ_* ($\rho_\odot$)	$0.45^{+0.23}_{-0.15}$	$0.67^{+0.16}_{-0.13}$	$0.323^{+0.035}_{-0.028}$
M_P ($M_{\rm Jup}$)	$0.490^{+0.059}_{-0.056}$	$0.496^{+0.064}_{-0.060}$	$0.498^{+0.059}_{-0.056}$
R_P ($R_{\rm Jup}$)	$1.74^{+0.26}_{-0.23}$	$1.51^{+0.10}_{-0.10}$	$1.97^{+0.10}_{-0.10}$
$\log g_P$ (cgs)	$2.56^{+0.14}_{-0.13}$	$2.696^{+0.086}_{-0.083}$	$2.466^{+0.051}_{-0.052}$
ρ_P (ρ_J)	$0.092^{+0.054}_{-0.032}$	$0.144^{+0.042}_{-0.031}$	$0.0648^{+0.0106}_{-0.0090}$
$T_{P,A=0}$ (K)	1662^{+113}_{-110}	1557^{+55}_{-55}	1756^{+26}_{-30}

Notes. Three solutions are presented (Cases 1, 2 and 3), each with different constraints as described in the text (Section 4).
[a] T_{58}: total eclipse duration.
[b] $T_{56} = T_{78}$: eclipse ingress/egress duration.

in accepted steps, the values of stellar radius are consistent with those of stellar mass for a main-sequence star: the probability distribution of R_* has a mean of $R_0 = M_0^{0.8}$ (Tingley & Sackett 2005), where R_0 is the initial estimate of R_*, and a standard deviation of $\sigma_R = 0.8(R_0/M_0)\sigma_M$. An initial MCMC analysis was used to determine stellar density, which was used as an input to an evolutionary analysis (Figure 5). This suggests a stellar mass of $1.19^{+0.07}_{-0.08}$ $M_\odot$ and a stellar age of $1.2^{+2.8}_{-1.2}$ Gyr. This stellar mass was used as the start value in the MCMC solution (Case 2) presented in the third column of Table 4. The MS prior results in a smaller stellar radius and, therefore, a smaller planetary radius ($R_P = 1.51 \pm 0.10$ $R_{\rm Jup}$). The MS prior on stellar radius, together with the prior on stellar mass, effectively places a prior on stellar density, ρ_*, forcing stellar density toward the higher values typical of a MS star. Therefore, as

$$\rho_* \propto \frac{(1-e^2)^{3/2}}{(1+e\sin\omega)^3}, \quad (1)$$

a more eccentric orbit ($e = 0.237^{+0.068}_{-0.069}$; $\omega = 278.0^{\circ+8.2}_{-5.6}$ deg) results. The uncertainties on each of the parameters affected by the MS prior are artificially small due to the MS prior not taking full account of uncertainties involved (e.g., in the theoretical mass–radius relationship).

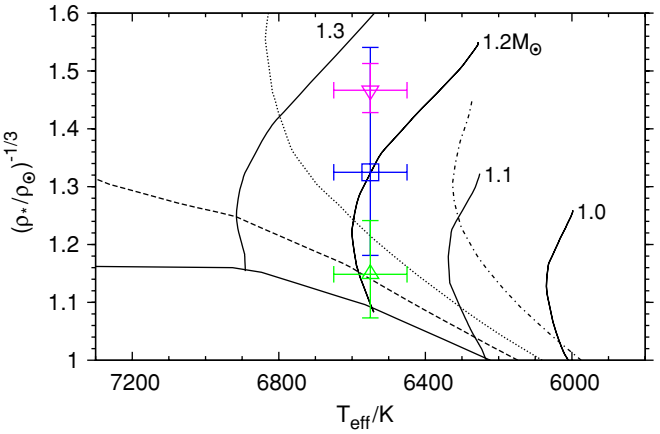

Figure 5. Modified H−R diagram: inverse cube root of stellar density vs. stellar effective temperature. The former quantity is purely observational, measured directly from the light curve in initial MCMC runs. The latter quantity is derived from the spectral analysis. The best-fitting values of the three models for WASP-17 are depicted using the key of Table 4. Evolutionary mass tracks (solid, labeled lines) and isochrones (100 Myr, solid; 1 Gyr, dashed; 2 Gyr, dotted; 4 Gyr, dot-dashed) from Girardi et al. (2000) for [Fe/H] = −0.25 are plotted for comparison.

(A color version of this figure is available in the online journal.)

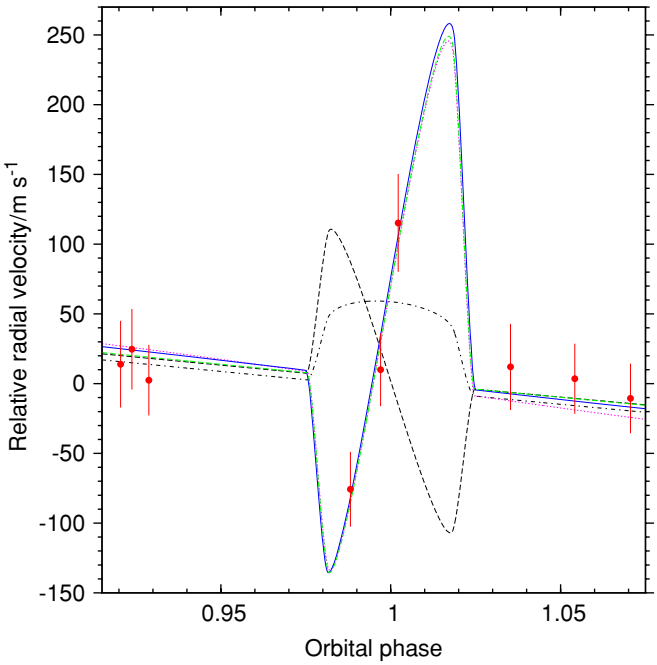

Figure 6. Zoom-in on the spectroscopic transit region of Figure 3, showing the fitted RM effect more clearly. The red circles are CORALIE measurements and the colored lines are the best-fitting models (Table 4). We show for comparison the RM effects that would result from perpendicular ($\lambda = -90°$; black, dot-dashed line) and aligned ($\lambda = 0°$; black, dashed line) spin–orbit axes; in both cases $v \sin i = 9.0$ km s^{-1} and $b = 0.355$ were fixed.

(A color version of this figure is available in the online journal.)

As the detection of a non-zero eccentricity in the first MCMC solution is of low significance, a third solution was generated, with an imposed circular orbit and no MS prior. Again, an initial MCMC analysis was performed to determine stellar density, which was used as an input to an evolutionary analysis (Figure 5). From that, a stellar mass of $1.25 \pm 0.08\ M_\odot$ and a stellar age of $3.1^{+1.1}_{-0.8}$ Gyr were found. This stellar mass was used as the start value in the MCMC solution (Case 3) presented in the fourth column of Table 4. The circular orbit causes the velocity of the planet during transit to be higher than in the two eccentric solutions. This results in a larger stellar radius and, as the depth of transit is fixed by measurement, in a larger planet radius ($R_P = 1.97 \pm 0.10\ R_{Jup}$).

For each model, the best-fitting transit light curve is shown in Figure 2, and the best-fitting RV curve is shown in Figure 3. To help decide between the three cases presented, a more precise determination of stellar age, stellar radius or orbtial eccentricity would be useful. It is currently difficult to reliably determine the age of stars older than 1–2 Gyr (e.g., Sozzetti et al. 2009 and references therein). Stellar radius could be calculated from a precise parallax determination. WASP-17's parallax is predicted to be 2.5 mas, which will be measurable to good precision by the forthcoming Gaia mission (Jordi et al. 2006), which is expected to achieve an accuracy of 7 μas at $V = 10$. Eccentricity can be better determined using a combination of two methods. (1) Take a number of high-precision RV measurements (which best constrain $e \sin \omega$), focusing on those phases at which the differences between the models are greatest (Figure 3). (2) Observe the secondary eclipse; the time of mid-eclipse constrains $e \cos \omega$ and the eclipse duration more weakly constrains $e \sin \omega$ (Charbonneau et al. 2005).

We adopt Case 1 as our preferred solution; we note that if WASP-17 proves to be young then Case 2 will be indicated, and Case 3 will be indicated if the planet's orbit is found to be (near-)circular.

4.1. A Retrograde Orbit?

The RM effect was incorporated in the MCMC analyses with free parameters $v \sin i \cos \lambda$ and $v \sin i \sin \lambda$ (Figure 6; Table 4). The three RV measurements during transit suggest a large spin–orbit misalignment ($\lambda \approx -150°$), indicating that the planet is orbiting in a sense counter to that of stellar rotation. The RV RMS about the fitted model is 31.6 m s^{-1}. Comparing a borderline prograde–retrograde orbit ($\lambda = -90°$, $v \sin i = 9.0$ km s^{-1}, $b = 0.355$), the first in-transit point is discrepant by 5.0σ, and the RV RMS is 40.2 m s^{-1} (Figure 6). Comparing a prograde orbit ($\lambda = 0°$, $v \sin i = 9.0$ km s^{-1}, $b = 0.355$), the first and third in-transit points are discrepant by 6.0σ and 3.8σ, respectively, and the RV RMS is 45.7 m s^{-1} (Figure 6).

The fitted amplitude of the RM effect suggests $v \sin i \approx 20$ km s^{-1}, which is higher than determined in the spectral analysis (Table 3). This could be because the amplitude of the RM effect is currently liable to be overestimated (Winn et al. 2005; Triaud et al. 2009) due to the manner in which the RVs are extracted from the spectra. At present, the effective velocity of the spectroscopic cross-correlation function (CCF) is measured by fitting a Gaussian. However, at values of $v \sin i$ significantly greater than the intrinsic width of the CCF for a slowly rotating star, the traveling bump in the profile that is the spectral signature of the planet's silhouette becomes partially resolved (Gaudi & Winn 2007). The CCF profile will become slightly asymmetric when the planet is near the limb, and this may bias the velocity measured by Gaussian-fitting to a greater value than the RV of the centroid of the unobscured parts of the star.

4.2. Transit Times

We measured the times of WASP-17b's transits to search for transit timing variations, as may be induced by a third body (e.g., Holman & Murray 2005; Agol et al. 2005). The model light curves were stepped in time over the photometric data

Table 5
Transit Times

N_{tr}	T_c (HJD)	σ_{T_c} (min)	$O-C$ (min)
−179	2453890.54850	6.2	16.6
−175	2453905.48193	5.5	4.7
−171	2453920.42243	3.6	2.8
−159	2453965.23733	5.0	−12.2
−96	2454200.57081	4.4	−11.2
−92	2454215.52194	2.7	2.3
−77	2454271.55701	4.1	7.2
−73	2454286.49409	8.3	0.5
−69	2454301.45133	8.2	22.8
−61	2454331.32310	9.3	5.8
−1	2454555.43662	6.4	−12.9
2	2454566.65046	8.3	−2.0
9	2454592.80049	0.55	0.79

around the predicted times of transit, and χ^2 was calculated at each step. The times of mid-transit were found by measuring the χ^2 minima, and the uncertainties were determined via bootstrapping. The calculated times of mid-transit, T_c, and the differences, $O-C$, between those times and the predicted times, assuming a fixed epoch and period (Table 4), are given in Table 5. No significant departure from a fixed ephemeris is seen.

5. DISCUSSION

WASP-17b is the least dense planet known, with a density of 0.06–0.14 ρ_J. TrES-4, the previous least dense planet, has a density of 0.15 ρ_J (Sozzetti et al. 2009), and HD 209458b, the most studied transiting planet, has a density of 0.27 ρ_J (Torres et al. 2008). WASP-17b's radius of 1.5–2 R_{Jup} is larger than predicted by standard planet evolution models. For example, those of Fortney et al. (2007) imply a radius of at most 1.3 R_{Jup} (the value for a 1 Gyr old, coreless planet of 0.41 M_{Jup}, receiving more stellar flux, at a distance of 0.02 AU, where each of these values errs on the side of inflating the radius).

Burrows et al. (2007) showed that an enhanced atmospheric opacity can delay radius shrinkage, leading to a larger-than-otherwise planet radius at a given age. Enhanced opacities may result from super-solar metallicity, the presence of clouds/hazes, or the effects of photolysis or non-equilibrium chemistry. One might expect a low planetary atmospheric opacity due to the sub-solar metallicity of the WASP-17 star: [Fe/H] = –0.25. However, as WASP-17b is highly irradiated, its atmospheric opacity is expected to be high due, for example, to the presence of TiO and VO gases (Burrows et al. 2008; Fortney et al. 2008). Ibgui & Burrows (2009) found that an atmospheric opacity of 3 × solar is sufficient to account for the radius of HD 209458b. The very large radius of WASP-17b and its moderate age suggest that enhanced opacity alone, even of 10 × solar, is insufficient to account for the planet's bloatedness.

It has been proposed (Bodenheimer et al. 2001; Gu et al. 2003; Jackson et al. 2008a) that tidal dissipation associated with the circularization of an eccentric orbit is able to substantially inflate the radius of a short-orbit, giant planet. If a planet is in a close ($a < 0.2$ AU), highly eccentric ($e > 0.2$) orbit then planetary tidal dissipation will be significant and will shorten and circularize the orbit. Orbital energy is deposited within the planet interior, leading to an inflated planet radius. This process is accelerated by higher atmospheric opacities: as the planet better retains heat, shrinking of the radius is retarded, and a larger radius causes greater tidal dissipation. Higher eccentricities result in stronger tides, and thus in greater tidal dissipation. The rate at which energy is tidally dissipated within a body is inversely proportional to its tidal quality factor, Q', which is the ratio of the energy in the tide to the tidal energy dissipated within the body per orbit (e.g., Ogilvie & Lin 2007).

Ibgui & Burrows (2009) created a tidal dissipation model and applied it to HD 209458b, which is bloated to a lesser degree than WASP-17b. A custom fit is required to find possible evolution histories for the WASP-17 system, but the similarity of HD 209458 (compare Tables 3 and 4 from this paper with Table 1 in Ibgui & Burrows (2009) and references therein) permits comparison. Ibgui & Burrows' (2009) HD 209458b model suggests that tidal heating could produce even WASP-17b's maximum likely radius ($R_P \approx 2\ R_{Jup}$) if, for example, it evolved from a highly eccentric ($e \approx 0.79$), close ($a \approx 0.085$ AU) orbit, with moderate tidal dissipation ($Q'_P \approx 10^{6.55}$; $Q'_* \approx 10^{7.0}$) and solar atmospheric opacity. The final semimajor axis of this particular model was shorter than that of WASP-17b, but within 10%. Such an eccentric, short orbit seems reasonable as planets in highly eccentric, quite short orbits are known: HD 17156b ($e = 0.676$, $a = 0.162$ AU; Winn et al. 2009d), HD 37605b ($e = 0.74$, $a = 0.26$ AU; Cochran et al. 2004), HD 80606b ($e = 0.934$, $a = 0.45$ AU; Moutou et al. 2009). As for the strength of tidal dissipation, Jackson et al. (2008b) found similar best-fitting values ($Q'_P = 10^{6.5}$; $Q'_* = 10^{5.5}$) when matching the current eccentricities of short-orbit ($a < 0.2$ AU) planets with the eccentricities of farther out planets, from which they presumably evolved.

The limited RV measurements during transit give a strong indication that WASP-17b is in a retrograde orbit. As the angular momenta of a star, its protoplanetary disk, and hence its planets, all derive from that of the parent molecular cloud, WASP-17b presumably originated in a prograde orbit. As a gas giant, WASP-17b is expected to have formed just outside the ice boundary (∼3 AU) and migrated inward to its current separation of 0.05 AU (e.g., Ida & Lin 2004). Migration of a giant planet via tidal interaction with a gas disk is expected to preserve spin–orbit alignment (Lin et al. 1996; Ward 1997) and is thus unable to produce a retrograde orbit. Alternatively, migration via a combination of star–planet scattering (Takeda et al. 2008) or planet–planet scattering (e.g., Rasio & Ford 1996; Chatterjee et al. 2008; Nagasawa et al. 2008) and tidal circularization of the resultant eccentric orbit is able to produce significant misalignment.

In addition to inclined orbits, scattering is able to produce highly eccentric orbits (e.g., Ford & Rasio 2008), which have been found to be common and are necessary if tidal circularization is to inflate planetary radii (e.g., Jackson et al. 2008b), whereas planet–disk interactions seem unable to pump eccentricities to large values ($e > 0.3$; D'Angelo et al. 2006). Nagasawa et al. (2008) carried out orbital integrations of three-planet systems: three Jupiter-mass planets were initially placed beyond the ice boundary (5 AU, 7.25 AU, 9.5 AU) in circular orbits, with small inclinations (0.°5, 1°, 1.°5), around a solar-mass star. They found that a combination of planet–planet scattering, the Kozai mechanism (the oscillation of the eccentricity and inclination of a planet's orbit via the secular perturbation from outer bodies; Kozai 1962), and tidal circularization produces short-orbit, giant planets in ∼30% of cases. The Kozai mechanism is most effective when the scattered, inner planet has an inclined orbit. A broad spread was seen in the inclination distribution of the short-orbit planets formed, including plan-

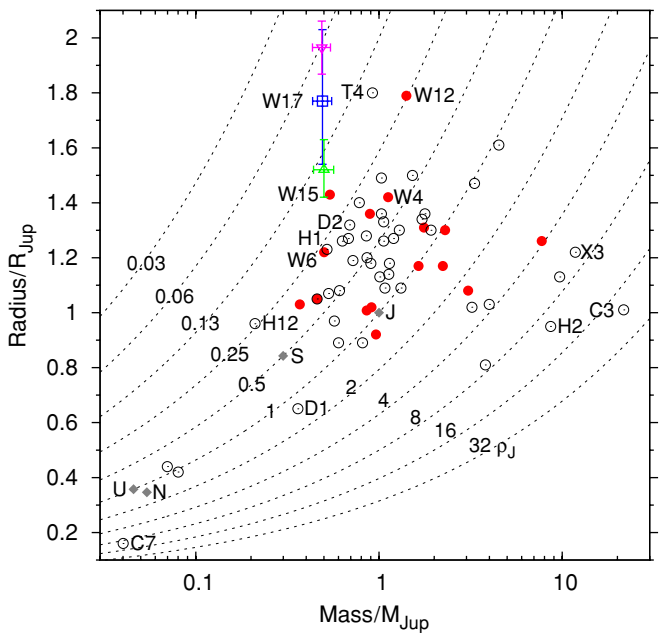

Figure 7. Mass–radius distribution of the 62 known transiting extrasolar planets. The best-fitting values for the three WASP-17b models are depicted according to the key given in Table 4. Other WASP planets are filled, red circles; non-WASP planets are open, black circles; Jupiter, Saturn, Neptune, and Uranus are filled, gray diamonds, labeled with the planets' initials. For clarity, error bars are displayed only for WASP-17b. Some planets discovered by *CoRoT*, HAT, TrES, WASP, and XO are labeled with the project initial and the system number (e.g., WASP-17b = W17). HD 149026b is labeled D1 and HD 209458b is labeled D2. The labeled, dashed lines depict a range of density contours in Jovian units. Data are taken from this work and http://exoplanet.eu.

(A color version of this figure is available in the online journal.)

ets in retrograde orbits. Therefore, we suggest that WASP-17b supports the hypothesis that some short-orbit, giant planets are produced by a combination of scattering, the Kozai mechanism, and tidal circularization. The observation of the RM effect for more short-orbit planets is required to measure the size of the contribution.

For planet–planet or star–planet scattering to have influenced WASP-17b's orbit in the past, one or more stellar or planetary companions must have been present in the system. Sensitive imaging could probe for a stellar companion, and further RV measurements are necessary to search for stellar or planetary companions. It will be worthwhile looking for long-term trends in the RVs to detect farther-out planets that might have been involved in past scattering. A straight-line fit to the residuals of the RV data about the model fits indicates no significant drift over a span of 622 days (e.g., for Case 1 the drift is -17 ± 11 m s^{-1}). In their three-planet integrations, Nagasawa et al. (2008) found that in 75% of cases one planet is ejected, a planet collides with the host star in 22% of cases, and two planets are ejected in 5% of cases. They also found that, since a small difference in orbital energy causes a large difference in semimajor axis in the outer region, the final semimajor axes of outer planets are widely distributed (peak at ∼15 AU, with a large spread). Therefore, it is possible that WASP-17 is now the only giant planet in the system or that the outer planets are in long orbits, which are difficult to detect with the RV technique.

The discovery of WASP-17b extends the mass–radius distribution of the 62 known transiting exoplanets (Figure 7). WASP-17b has the largest atmospheric scale height (1100–2100 km) of any known planet by up to a factor 2, due to its very low surface gravity and moderately high equilibrium temperature. The ratio of projected areas of planetary atmosphere to stellar disk of WASP-17b is 1.9–2.7 times that of HD 209458b and 2.4–3.4 times that of HD 189733b, for both of which successful attempts at measuring atmospheric signatures have been made (e.g., Charbonneau et al. 2002; Desert et al. 2009). Thus, although WASP-17 is fainter and has a larger stellar radius, the system is a good prospect for transmission spectroscopy.

We acknowledge a thorough and constructive report from the anonymous referee. The WASP consortium comprises the Universities of Keele, Leicester, St. Andrews, the Queen's University Belfast, the Open University and the Isaac Newton Group. WASP-South is hosted by the South African Astronomical Observatory and we are grateful for their support and assistance. Funding for WASP comes from consortium universities and from the UK's Science and Technology Facilities Council.

REFERENCES

Agol, E., Steffen, J., Sari, R., & Clarkson, W. 2005, MNRAS, 359, 567
Bakos, G. A., et al. 2007, ApJ, 656, 552
Baranne, A., et al. 1996, A&AS, 119, 373
Bodenheimer, P., Lin, D. N. C., & Mardling, R. A. 2001, ApJ, 548, 466
Böhm-Vitense, E. 2004, AJ, 128, 2435
Burrows, A., Budaj, J., & Hubeny, I. 2008, ApJ, 678, 1436
Burrows, A., Hubeny, I., Budaj, J., & Hubbard, W. B. 2007, ApJ, 661, 502
Charbonneau, D., Brown, T. M., Latham, D. W., & Mayor, M. 2000, ApJ, 529, L45
Charbonneau, D., Brown, T. M., Noyes, R. W., & Gilliland, R. L. 2002, ApJ, 568, 377
Charbonneau, D., et al. 2005, ApJ, 626, 523
Chatterjee, S., Ford, E. B., Matsumura, S., & Rasio, F. A. 2008, ApJ, 686, 580
Cochran, W. D., et al. 2004, ApJ, 611, L133
Collier Cameron, A., et al. 2006, MNRAS, 373, 799
Collier Cameron, A., et al. 2007, MNRAS, 380, 1230
D'Angelo, G., Lubow, S. H., & Bate, M. R. 2006, ApJ, 652, 1698
Desert, J.-M., Lecavelier des Etangs, A., Hebrard, G., Sing, D. K., Ehrenreich, D., Ferlet, R., & Vidal-Madjar, A. 2009, ApJ, 699, 478
Fabrycky, D. C., & Winn, J. N. 2009, ApJ, 696, 1230
Ford, E. B. 2006, ApJ, 642, 505
Ford, E. B., & Rasio, F. A. 2008, ApJ, 686, 621
Fortney, J. J., Lodders, K., Marley, M. S., & Freedman, R. S. 2008, ApJ, 678, 1419
Fortney, J. J., Marley, M. S., & Barnes, J. W. 2007, ApJ, 659, 1661
Gaudi, B. S., & Winn, J. N. 2007, ApJ, 655, 550
Gillon, M. 2009, arXiv:0906.4904
Gillon, M., Pont, F., Moutou, C., Bouchy, F., Courbin, F., Sohy, S., & Magain, P. 2006, A&A, 459, 249
Gillon, M., et al. 2009a, A&A, 496, 259
Gillon, M., et al. 2009b, A&A, 501, 785
Girardi, L., Bressan, A., Bertelli, G., & Chiosi, C. 2000, A&AS, 141, 371
Gray, D. F. 2008, The Observation and Analysis of Stellar Photospheres (3rd ed; Cambridge: Cambridge Univ. Press)
Gu, P.-G., Lin, D. N. C., & Bodenheimer, P. H. 2003, ApJ, 588, 509
Guillot, T., & Showman, A. P. 2002, A&A, 385, 156
Guillot, T., Santos, N. C., Pont, F., Iro, N., Melo, C., & Ribas, I. 2006, A&A, 453, L21
Hebb, L., et al. 2008, ApJ, 693, 1920
Hebb, L., et al. 2010, ApJ, 708, 224
Hébrard, G., et al. 2008, A&A, 488, 763
Henry, G. W., Marcy, G. W., Butler, R. P., & Vogt, S. S. 2000, ApJ, 529, L41
Holman, M. J., & Murray, N. W. 2005, Science, 307, 1288
Ibgui, L., & Burrows, A. 2009, ApJ, 700, 1921
Ida, S., & Lin, D. N. C. 2004, ApJ, 604, 388
Jackson, B., Greenberg, R., & Barnes, R. 2008a, ApJ, 681, 1631
Jackson, B., Greenberg, R., & Barnes, R. 2008b, ApJ, 678, 1396
Johnson, J. A., et al. 2008, ApJ, 686, 649
Johnson, J. A., et al. 2009, PASP, 121, 1104
Johns-Krull, C. M., et al. 2008, ApJ, 677, 657
Jordi, C., et al. 2006, MNRAS, 367, 290
Joshi, Y. C., et al. 2009, MNRAS, 392, 1532
Knutson, H. A., Charbonneau, D., Burrows, A., O'Donovan, F. T., & Mandushev, G. 2009, ApJ, 691, 866

Knutson, H. A., Charbonneau, D., Noyes, R. W., Brown, T. M., & Gilliland, R. L. 2007, ApJ, 655, 564
Kozai, Y. 1962, AJ, 67, 591
Lin, D. N. C., Bodenheimer, P., & Richardson, D. C. 1996, Nature, 380, 606
Mandushev, G., et al. 2007, ApJ, 667, L195
Mayor, M., Pepe, F., & Queloz, D. 2003, Messenger, 114, 20
Moutou, C., et al. 2009, A&A, 498, L5
Nagasawa, M., Ida, S., & Bessho, T. 2008, ApJ, 678, 498
Ogilvie, G. I., & Lin, D. N. C. 2007, ApJ, 661, 1180
Pepe, F., et al. 2005, Messenger, 120, 22
Pollacco, D., et al. 2006, PASP, 118, 1407
Pollacco, D., et al. 2008, MNRAS, 385, 1576
Pont, F., et al. 2009, A&A, 502, 695
Queloz, D., Eggenberger, A., Mayor, M., Perrier, C., Beuzit, J. L., Naef, D., Sivan, J. P., & Udry, S. 2000a, A&A, 359, L13
Queloz, D., et al. 2000b, A&A, 354, 99
Queloz, D., et al. 2001, A&A, 379, 279
Rasio, F. A., & Ford, E. B. 1996, Science, 274, 954
Southworth, J., et al. 2009, MNRAS, 399, 287
Sozzetti, A., et al. 2009, ApJ, 691, 1145
Takeda, G., Kita, R., & Rasio, F. A. 2008, ApJ, 683, 1063
Tingley, B., & Sackett, P. D. 2005, ApJ, 627, 1011
Torres, G., et al. 2008, ApJ, 677, 1324
Triaud, A. H. M. J., et al. 2009, A&A, 506, 377
Ward, W. R. 1997, Icarus, 126, 261
West, R. G., et al. 2009, AJ, 137, 4834
Wilson, D. M., et al. 2008, ApJ, 675, L113
Winn, J. N., Holman, M. J., Carter, J. A., Torres, G., Osip, D. J., & Beatty, T. 2009a, AJ, 137, 3826
Winn, J. N., et al. 2005, ApJ, 631, 1215
Winn, J. N., et al. 2007, AJ, 134, 1707
Winn, J. N., et al. 2008, ApJ, 683, 1076
Winn, J. N., et al. 2009b, ApJ, 700, 302
Winn, J. N., et al. 2009c, ApJ, 703, 2091
Winn, J. N., et al. 2009d, ApJ, 693, 794